●●●

The elasticity of the MgSiO₃ post-perovskite phase in the Earth's lowermost mantle

T. Iitaka[1], K. Hirose[2], K. Kawamura[2] & M. Murakami[2]

[1]*Computational Astrophysics Laboratory, RIKEN (The Institute of Physical and Chemical Research), 2-1 Hirosawa, Wako, Saitama 351-0198, Japan*
[2]*Department of Earth and Planetary Sciences, Tokyo Institute of Technology, 2-12-1 Ookayama, Meguro, Tokyo 152-8551, Japan*

MgSiO₃ perovskite has been assumed to be the dominant component of the Earth's lower mantle, although this phase alone cannot explain the discontinuity in seismic velocities observed 200–300 km above the core–mantle boundary (the D″ discontinuity) or the polarization anisotropy observed in the lowermost mantle[1]. Experimental and theoretical studies that have attempted to attribute these phenomena to a phase transition in the perovskite phase have tended to simply confirm the stability of the perovskite phase[2–6]. However, recent *in situ* X-ray diffraction measurements have revealed[7] a transition to a 'post-perovskite' phase above 125 GPa and 2,500 K—conditions close to those at the D″ discontinuity. Here we show the results of first-principles calculations of the structure, stability and elasticity of both phases at zero temperature. We find that the post-perovskite phase becomes the stable phase above 98 GPa, and may be responsible for the observed seismic discontinuity and anisotropy in the lowermost mantle. Although our ground-state calculations of the unit cell do not include the effects of temperature and minor elements, they do provide a consistent explanation for a number of properties of the D″ layer.

The first-principles calculations were performed with the initial models of the perovskite and post-perovskite phases, which are the orthorhombic unit cells containing four molecules with the space group *Pbnm* and *Cmcm*, respectively (Fig. 1). Then the lattice constants and the positions of the atoms were optimized within the given symmetry to minimize the enthalpy (see Methods). This procedure was repeated by changing the external pressure from 80 GPa to 130 GPa in steps of 10 GPa. It was found that the post-perovskite phase becomes the stable phase above 98 GPa at $T = 0$ K by drawing a graph of the enthalpy difference $\Delta H = H(\text{PP}) - H(\text{Pv})$ as a function of pressure (Fig. 2). (Here we use PP to indicate a property of the post-perovskite phase, and Pv a property of the perovskite phase.)

Table 1 lists the parameters of the optimized structures of the post-perovskite and perovskite phases at 120 GPa, together with the experimental data[7]. The coordination numbers of Mg and Si in the post-perovskite phase are same as those in the perovskite phase—namely, eight for Mg and six for Si. The principal difference between the two structures is the linkage of SiO₆ octahedra. In the post-perovskite phase, they share edges, thereby forming chains, and the chains share the octahedral corners thereby forming flat sheets[7], whereas in the perovskite phase, the octahedra share corners, thereby forming a three-dimensional network. The average Si–O distance of the post-perovskite phase (1.665 Å) is longer than that of the perovskite phase (1.650 Å); on the other hand, the average Mg–O distance of the post-perovskite phase (1.959 Å) is shorter than that of the perovskite phase (1.981 Å). The reduction of the Mg–O polyhedra and both the edge sharing and deformation of the SiO₆ octahedra cause a volume reduction of the post-perovskite phase from that of the perovskite phase. The small space for cations suggests that Mg, which is a very small cation, is much more comfortable in post-perovskite phase than other cations. Our first-principles calculations show that the post-perovskite phase is about 1.4% denser than the perovskite phase throughout the pressure range, which is in agreement with the experimental value[7] of 1.0–1.2% at 120 GPa and 300 K.

The post-perovskite phase of MgSiO₃ (Fig. 1b) is isostructural with UFeS₃, UFeSe₃, ThMnTe₃, ThMgTe₃, UMnSe₃ and ThMnSe₃ (refs 8–10). The crystal habit of ThMnTe₃ and ThMgTe₃ was reported[9] to be platy (and needle-like). Although the crystallographic direction was not mentioned in the literature, the surface of the plate should be the (010) surface, which is parallel to the sheet structure, and the direction of the needle should be the [100] direction, which is the direction of the edge-shared octahedral chain. There is an important difference between the post-perovskite phase of MgSiO₃ and those of $\text{Th}^{(IV)}\text{Mn}^{(II)}\text{Te}_3^{(II)}$ and $\text{Th}^{(IV)}\text{Mg}^{(II)}\text{Te}_3^{(II)}$: the eight-coordinated Mg–O bonds are weaker than $\text{Th}^{(IV)}$–$\text{Te}^{(II)}$ and the octahedral Si–O bonds are stronger than $\text{Mn}^{(II)}$–$\text{Te}^{(II)}$ and $\text{Mg}^{(II)}$–$\text{Te}^{(II)}$. These bonding features imply that the inter-chain bonds of the MgSiO₃ post-perovskite phase are much stronger than those of the ThMnTe₃ and ThMgTe₃ post-perovskite phase, and that the MgSiO₃ post-perovskite phase most probably has the platy crystal habit with (010) facets. The system of uranium transition-metal chalcogenides UMS₃ and UMSe₃ (where M is a transition metal) also shows an interesting relation to the perovskite–post-perovskite phase transition, because the structure of these compounds changes when M changes, instead of when the pressure changes: UMS₃ ($M = $ V, Cr, Co, Ni, Ru, Rh) and UMSe₃ ($M = $ V, Cr, Co, Ni) take the *Pbnm* structure, and UMnSe₃, UFeSe₃ and UFeS₃ take the *Cmcm* structure. The mechanism behind this
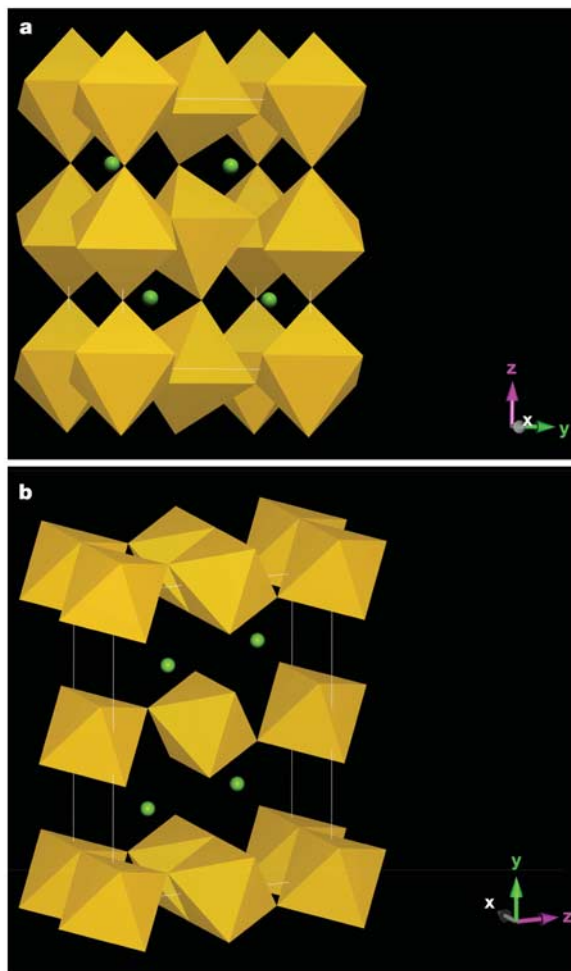

Figure 1 The unit cell structures of MgSiO₃. **a**, Perovskite; **b**, post-perovskite. The spheres represent Mg, and the octahedra represent Si with sixfold oxygen coordination.

structure change is still unknown[10].

Table 2 shows the nine elastic stiffness constants c_{ij} evaluated by the first-principles calculations. The crystal of the post-perovskite phase is much more compressible along the b-axis than along the a- or c-axis as $c_{22} \ll c_{11}, c_{33}$ (see also Supplementary Fig. 1), which could be a significant source of its seismic anisotropy. The propagation direction ($\mathbf{n}$) dependence of the seismic wave velocities in the perovskite and post-perovskite phase at the phase boundary ($\sim$100 GPa) were evaluated by solving the Christoffel equation $\det\left|c_{ijkl}n_j n_l - \rho V^2 \delta_{ik}\right| = 0$ for the single crystal (Fig. 3). The wave velocities vary significantly with the propagation direction and the polarization, suggesting that both the phases exhibit strong anisotropy in both compressional (P) and shear (S) waves. The particular softness of the post-perovskite phase along the b-axis is reflected in the velocity minima when the polarization is along the b-axis, that is, when the propagation direction is along [010] for P waves or along [100] and [001] for S waves. A measure of anisotropy may be defined[11,12] by $A = (v_{max} - v_{min})/\langle v \rangle \times 100\%$, where v_{max} and v_{min} are the maximum and minimum velocities, respectively, and $\langle v \rangle$ is the velocity for an isotropic aggregate of crystal calculated from the c_{ij} by the Voigt-Reuss-Hill averaging scheme[1]. Though both the phases show strong anisotropy, the post-perovskite phase is found more anisotropic than the perovskite phase: the azimuth anisotropy of P and S waves is $A_P = 16\%$ and $A_S = 31\%$ for the post-perovskite phase, whereas $A_P = 11\%$ and $A_S = 16\%$ for the perovskite phase.

The D″ discontinuity is observed[13] in many regions around the world about 200–300 km above the core–mantle boundary with an increase of up to 3.0% in both S- and P-wave velocities. On the basis of global seismic tomography, Sidorin[14] proposed a model of a possibly ubiquitous seismic discontinuity atop the D″ layer that is caused by a solid–solid phase transition with a Clapeyron slope of $6 \, \text{MPa K}^{-1}$. The increase of seismic velocities atop the D″ layer is attributed to the increase of bulk (K) and shear (G) moduli at the transition, which overcomes the increase of the density. One of the weak points of this model was that no relevant phase transition had been observed in the major constituents of the lower mantle, $MgSiO_3$ perovskite and magnesiowüstite. Therefore the discovery of the post-perovskite phase transition above 125 GPa and 2,500 K by Murakami et al.[7] provides a strong ground for the model. The phase boundary drawn with the transition pressures at $T = 0 \, \text{K}$ (from the first-principles calculation) and at $T = 2,500 \, \text{K}$ (from the high-pressure experiments) has a Clapeyron slope of $10 \, \text{MPa K}^{-1}$, which is close to Sidorin's value.

In the D″ layer significant polarization anisotropy has been reported[15,16], especially under the circum-Pacific regions, where the horizontally polarized S-wave velocity (v_{SH}) is 1–3% faster than the vertically polarized S-wave velocity (v_{SV}). The post-perovskite phase transition can explain why the polarization anisotropy is observed only in the D″ layer but not in the overlying mantle[15]. In the possible horizontal shear flow in the D″ layer, crystals of the post-perovskite phase are probably preferentially oriented with the most compressible b-axis in the vertical direction. This seems very likely because the crystal of the post-perovskite phase has the sheet stacking structure along the b-axis (Fig. 1b). Therefore we modelled the phase boundary by using an isotropic aggregate of perovskite phase and a transversely isotropic aggregate of post-perovskite phase with the b-axis as the symmetry axis. Then we calculated the seismic wave velocities at the phase boundary by using the Voigt-Reuss-Hill averaging scheme for the perovskite phase, and the scheme of refs 17 and 18 for the velocities of the horizontally propagating P wave ($v_{PH}^{(PP)}$) and the horizontally and vertically polarized S-waves ($v_{SH}^{(PP)}$, $v_{SV}^{(PP)}$) in the post-perovskite phase. The discontinuities in P and S waves are estimated as 4–7% or $v_{PH}^{(PP)}/\langle v_P^{(Pv)} \rangle = 1.04$, $v_{SH}^{(PP)}/\langle v_S^{(Pv)} \rangle = 1.07$, and $v_{SV}^{(PP)}/\langle v_S^{(Pv)} \rangle = 1.03$. The polarization anisotropy of S waves in the post-perovskite phase is estimated as 4% or $v_{SH}^{(PP)}/v_{SV}^{(PP)} = 1.04$. This result may be regarded as consistent with the observations[13,14] if we consider the effect of imperfect crystal alignments. With isotropic aggregates of the post-perovskite phase, very small discontinuities, $\langle v_P^{(PP)} \rangle / \langle v_P^{(Pv)} \rangle = 0.999$ and $\langle v_S^{(PP)} \rangle / \langle v_S^{(Pv)} \rangle = 1.01$, and no anisotropy are expected. Our model is in contrast to the model with the preferentially oriented perovskite phase where the most compressible axis becomes horizontal, and therefore the wrong polarization anisotropy, $v_{SV} > v_{SH}$, occurs[18,19].

Moreover, anti-correlation between bulk-sound velocity and S-wave velocity has been observed in the very deep portions of the mantle[20]. The present results show slower bulk-sound velocity and
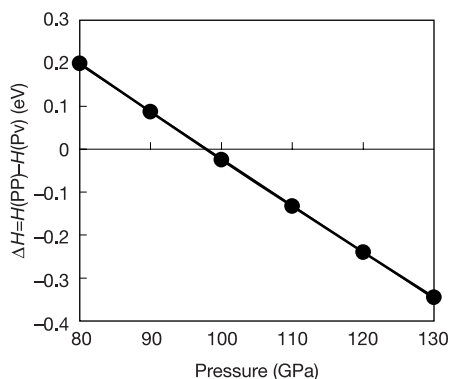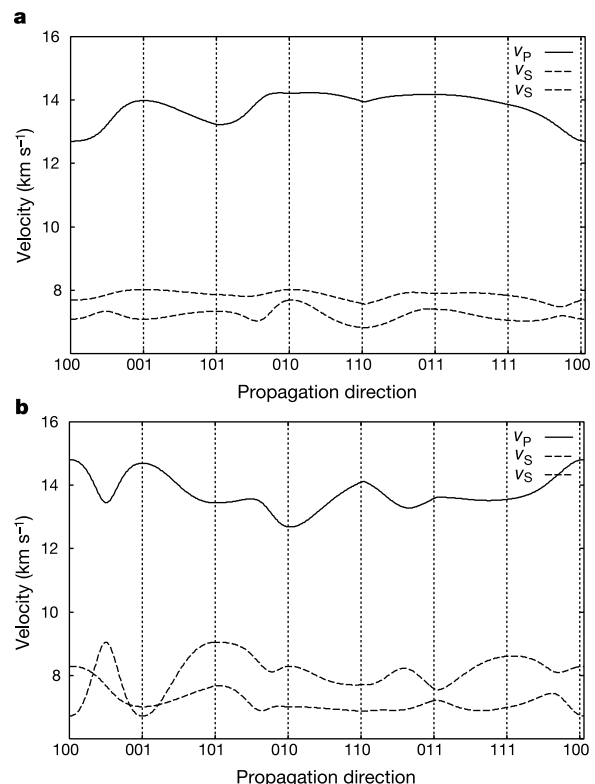
Figure 2 The enthalpy difference between the perovskite phase and post-perovskite phase as a function of pressure. The post-perovskite (PP) phase is favoured over the perovskite (Pv) phase at pressures above 98 GPa.

Figure 3 The variation of compressional (v_P) and shear (v_S) wave velocities as a function of propagation direction. **a**, Perovskite phase at 100 GPa; **b**, post-perovskite phase at 100 GPa. The two dashed lines represent the two polarizations of the shear waves.

Table 1 Crystal data of post-perovskite and perovskite phases

	Coordinate	Post-perovskite phase Experimental[7] (121 GPa, 300 K)	Post-perovskite phase Calculated (120 GPa, 0 K)	Perovskite phase Calculated (120 GPa, 0 K)
Crystal system		Orthorhombic	Orthorhombic	Orthorhombic
Space group		$Cmcm$ (no. 63)	$Cmcm$	$Pbnm$ (no. 62)
Cell parameters				
a (Å)		2.456	2.455	4.289
b (Å)		8.042	8.051	4.557
c (Å)		6.093	6.099	6.264
Z		4	4	4
V (Å³)		120.39	120.55	122.43
Atomic coordinates				
Mg (4c)	x	0.0	0.0	0.477
	y	0.253	0.253	0.925 (4c)
	z	0.25	0.25	0.25
Si (4a)	x	0.0	0.0	0.0
	y	0.0	0.0	0.0 (4a)
	z	0.0	0.0	0.0
O1 (4c)	x	0.0	0.0	0.884
	y	0.923	0.928	0.033 (4c)
	z	0.25	0.25	0.25
O2 (8f)	x	0.0	0.0	0.817
	y	0.631	0.636	0.307 (8d)
	z	0.436	0.442	0.557
Interatomic distances (Å)				
Si–O			1.632(× 2), 0.681(× 4)	1.645(× 2),1.649(× 2) 1.657(× 2)
Average			[1.665]	[1.650]
O–O edges			2.296, 2.305, 2.327, 2.337, 2.380, 2.456	2.313, 2.321, 2.330, 2.346, 2.347, 2.349, 2.415, 2.464
Mg–O			1.867(× 2), 1.943(× 4) 2.084(× 2)	1.815, 1.848(× 2), 1.885, 2.042(× 2) 2.185(× 2)
Average			[1.959]	[1.981]
Shortest Si–Si			2.455	3.129
Si–Mg			2.547	2.494
Mg–Mg			2.455	2.997

Table 2 The elastic-stiffness constants c_{ij} of post-perovskite and perovskite phases

	c_{11}	c_{22}	c_{33}	c_{12}	c_{13}	c_{23}	c_{44}	c_{55}	c_{66}	K	G
Post-perovskite phase											
100 GPa	1175	862	1157	366	289	437	264	242	368	595	306
120 GPa	1270	937	1264	425	329	493	291	264	412	660	332
Perovskite phase											
100 GPa	852	1068	1033	461	368	391	340	265	312	596	296
120 GPa	909	1160	1128	520	410	434	363	278	339	654	314
Perovskite phase[18]											
100 GPa	926	1160	1056	460	380	406	360	265	330	623	314
120 GPa	996	1263	1156	530	415	449	388	279	360	682	337

The values of Wentzcovitch[18] are interpolated to third-order polynomials by using the data at five different pressures listed in their paper.

faster S-wave velocity for the post-perovskite phase than for the perovskite phase at equivalent pressure, suggesting that such negative correlation may be accounted for by the heterogeneity in the mineral proportion of the perovskite phase and the post-perovskite phase. It is, however, noted that the present calculations were made at $T = 0$ K and for the Mg end-member composition. The effects of temperature[21,22] and the solution of minor elements were neglected here. The experiments on natural pyrolitic mantle composition showed that the $MgSiO_3$-rich post-perovskite contains much less iron than the perovskite[23], in accordance with our 'space for cations' argument. □

Methods

Our first-principles calculations were performed with CASTEP 4.2 codes based on the plane wave basis set, the Vanderbilt-type ultrasoft pseudopotentials[24–26] for electron–ion interaction, and the local density approximation (LDA) for exchange-correlation interaction. Previous studies[11,12,18,26] show that such a method reproduces very well the structures and properties of silicates under high pressure. The Brillouin zones are sampled with $6 \times 4 \times 4$ Monkhorst-Pack k-points[27] for the perovskite phase and $8 \times 2 \times 4$ k-points for the post-perovskite phase by using the maximal symmetry of the model. Increasing the number of k-points to $6 \times 6 \times 4$ and $10 \times 4 \times 4$, respectively, changes the total energy only 10^{-5} eV per atom. The cut-off energy is set to 800 eV; increasing the cut-off energy to 1,600 eV changes the enthalpy difference of the two phases by only 10^{-3} eV per atom. During the structural optimization, the enthalpy $H = E + PV$ is minimized by varying cell shape and atomic positions under the restriction of the given symmetry. In the geometrical optimization, the total stress tensor[28] is reduced to the order of 0.01 GPa by using the finite basis-set corrections[29]. The nine elastic stiffness constants c_{ij} are evaluated by computing the stress tensor σ_i generated by forcing strain ϵ_j to the optimized unit cell with four different magnitudes, $\epsilon = -0.02, -0.01, 0.01$ and 0.02, and by fitting them to the third-order polynomial of ϵ to remove the nonlinear contributions[11,12,30].

1. Poirier, J. P. *Introduction to the Physics of the Earth's Interior* (Cambridge Univ. Press, Cambridge, 2000).
2. Fiquet, G., Dewaele, A., Andrault, D., Kunz, M. & Le Bihan, T. Thermoelastic properties and crystal structure of MgSiO₃ perovskite at lower mantle pressure and temperature conditions. *Geophys. Res. Lett.* **27,** 21–24 (2000).
3. Andrault, D. Evaluation of (Mg, Fe) partitioning between silicate perovskite and magnesiowustite up to 120 GPa and 2300 K. *J. Geophys. Res.* **106,** 2079–2087 (2001).
4. Stixrude, L. & Cohen, R. E. Stability of orthorhombic MgSiO₃ perovskite in the Earth's lower mantle. *Nature* **364,** 613–616 (1993).
5. Wentzcovitch, R. M., Ross, N. L. & Price, G. D. Ab initio study of MgSiO₃ and CaSiO₃ perovskites at lower-mantle pressures. *Phys. Earth Planet. Inter.* **90,** 101–112 (1995).
6. Warren, M. C., Ackland, G. J., Karki, B. B. & Clark, S. J. Phase transitions in silicate perovskites from first principles. *Mineral. Mag.* **62,** 585–598 (1998).
7. Murakami, M., Hirose, K., Kawamura, K., Sata, N. & Ohishi, Y. Post-perovskite phase transition in MgSiO₃. *Science* **304,** 855–858 (2004).
8. Noel, H. & Padiou, J. Structure crystalline de FeUS₃. *Acta Crystallogr. B* **32,** 1593–1595 (1976).
9. Narducci, A. A. & Ibers, J. A. The related compounds MThTe₃(M = Mn, Mg) and ACuThSe₃(A = K, Cs): Syntheses and characterization. *Inorg. Chem.* **39,** 688–691 (2000).
10. Ijjaali, I., Mitchell, K., Huang, F. Q. & Ibers, J. A. Syntheses and characterization of the actinide manganese selenides ThMnSe₃ and UMnSe₃. *J. Solid State Chem.* **177,** 257–261 (2004).
11. Karki, B. B. *et al.* Structure and elasticity of MgO at high pressure. *Am. Mineral.* **82,** 51–60 (1997).
12. Karki, B. B. *et al.* Elastic properties of orthorhombic MgSiO₃ perovskite at lower mantle pressures. *Am. Mineral.* **82,** 635–638 (1997).

13. Wysession, M. E., *et al.* in *The Core-Mantle Boundary Region* (eds Gurnis, M., Wysession, M. E., Knittle, E. & Buffett, B. A.) 273–297 (American Geophysical Union, Washington DC, 1998).

14. Sidorin, I., Gurnis, M. & Helmberger, D. V. Evidence for a ubiquitous seismic discontinuity at the base of the mantle. *Science* **286**, 1326–1331 (1999).

15. Lay, T., Williams, Q., Garnero, E. J., Kellogg, L. & Wysession, M. E. in *The Core-Mantle Boundary Region* (eds Gurnis, M., Wysession, M. E., Knittle, E. & Buffett, B. A.) 299–318 (American Geophysical Union, Washington DC, 1998).

16. Panning, M. & Romanowicz, B. Inferences on flow at the base of Earth's mantle based on seismic anisotropy. *Science* **303**, 351–353 (2004).

17. Montagner, J. P. & Nataf, H. C. A simple method for inverting the azimuthal anisotropy of surface waves. *J. Geophys. Res.* **91**, 511–520 (1986).

18. Wentzcovitch, R. M., Karki, B. B., Karato, S. & Da Silva, C. R. S. High pressure elastic anisotropy of MgSiO3 perovskite and geophysical implications. *Earth Planet. Sci. Lett.* **164**, 371–378 (1998).

19. Karato, S., Zhang, S. & Wenk, H. R. Superplasticity in Earth's lower mantle: evidence from seismic anisotropy and rock physics. *Science* **270**, 458–461 (1995).

20. Masters, G. & Laske, G. in *Earth's Deep Interior: Mineral Physics and Tomography from the Atomic to the Global Scale* (eds Karato, S., Forte, A., Liebermann, R., Masters, G. & Stixrude, L.) 63–87 (American Geophysical Union, Washington DC, 2000).

21. Oganov, A. R., Brodholt, J. P. & Price, G. D. The elastic constants of MgSiO3 perovskite at pressures and temperatures of the Earth's mantle. *Nature* **411**, 934–937 (2001).

22. Wentzcovitch, R. M., Karki, B. B., Cococcioni, M. & de Gironcoli, S. Thermoelastic properties of MgSiO3-perovskite: insights on the nature of the Earth's lower mantle. *Phys. Rev. Lett.* **92**, 018501 (2004).

23. Murakami, M. *Phase Transition of Lower Mantle Mineral and its Geophysical Implications* Thesis, Tokyo Institute of Technology (2004).

24. Vanderbilt, D. Soft self-consistent pseudopotentials in a generalized eigenvalue formalism. *Phys. Rev. B* **41**, 7892–7895 (1990).

25. Civalleri, B. & Harrison, N. M. New ultrasoft pseudopotentials for the study of silicates. *Mol. Simulat.* **28**, 213–237 (2002).

26. Brodholt, J. P., Organov, A. R. & Price, G. D. Computational mineral physics and the physical properties of perovskite. *Phil. Trans. R. Soc. Lond. A* **360**, 2507–2520 (2002).

27. Monkhorst, H. J. & Pack, J. D. Special points for Brillouin-zone integrations. *Phys. Rev. B* **13**, 5188–5192 (1976).

28. Nielsen, O. H. & Martin, R. M. First principles calculation of stress. *Phys. Rev. Lett.* **50**, 697–700 (1983).

29. Francis, G. P. & Payne, M. C. Finite basis set corrections to total energy pseudopotential calculations. *J. Phys. Condens. Matter* **2**, 4395–4404 (1990).

30. Iitaka, T. & Ebisuzaki, T. First-principles calculation of elastic properties of solid argon at high pressures. *Phys. Rev. B* **65**, 012103 (2002).

temperatures of the D″ layer, MgSiO3 transforms from perovskite into a layered CaIrO3-type post-perovskite phase. The elastic properties of the post-perovskite phase and its stability field explain several observed puzzling properties of the D″ layer: its seismic anisotropy[2], the strongly undulating shear-wave discontinuity at its top[3–6] and possibly the anticorrelation between shear and bulk sound velocities[7,8].

If MgSiO3 perovskite is stable throughout the lower mantle, it should be the most abundant mineral in our planet. While some researchers[9] have suggested its decomposition into the oxides at lower mantle conditions, most workers[10–13] have found that perovskite is more stable than the oxides. To our knowledge, the possibility that MgSiO3 could be stable in a completely new structure within the lower mantle has not been considered.

The shear-wave discontinuity at the top of the D″ layer, suggested in ref. 3, has a strong topography. This discontinuity has commonly been explained by some chemical difference between the D″ layer and the rest of the lower mantle. However, using a combination of dynamical and seismic modelling, Sidorin *et al.*[4–6] have shown that the most consistent explanation is a phase transition in mantle minerals. Their best model[5,6] had a shear-wave discontinuity of ~1% located ~150 km above the core–mantle boundary (depth 2,740 km), with a Clapeyron slope of $6\,MPa\,K^{-1}$ (though values as large as $10\,MPa\,K^{-1}$ were almost equally acceptable). The discontinuities of the compressional wave velocities and of the density could not be resolved. The models of Sidorin *et al.*[4–6] were very appealing, but the major problem was that no appropriate phase transition was known at the time. Here we show that MgSiO3 perovskite undergoes a structural phase transition at the conditions corresponding to the top of the D″ layer. The predicted seismic signatures of this transition match the seismological inferences of Sidorin *et al.*[4–6].

A key observation made by Ono *et al.*[14] was that Fe_2O_3, like MgSiO3, transforms from the corundum (or ilmenite) to the perovskite structure under pressure. As these authors further found[14], a post-perovskite phase of Fe_2O_3 with a CaIrO3-type *Cmcm* structure[15] (Fig. 1) is stable above 60 GPa. This has led to the idea that a similar structure could be stable for MgSiO3 at high pressure.

We explored this idea using *ab initio* simulations based on density functional theory within the local density approximation
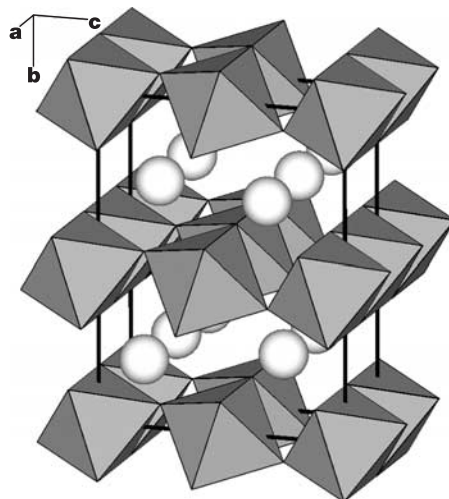
Theoretical and experimental evidence for a post-perovskite phase of MgSiO₃ in Earth's D″ layer

Artem R. Oganov[1] & **Shigeaki Ono**[2]

[1]*Laboratory of Crystallography, Department of Materials, ETH Zurich, Wolfgang Pauli Strasse 10, CH-8093 Zurich, Switzerland*
[2]*Institute for Frontier Research on Earth Evolution, Japan Agency for Marine-Earth Science and Technology, 2-15 Natsushima-cho, Yokosuka-shi, Kanagawa 237-0061, Japan*

The Earth's lower mantle is believed to be composed mainly of (Mg,Fe)SiO3 perovskite, with lesser amounts of (Mg,Fe)O and CaSiO3 (ref. 1). But it has not been possible to explain many unusual properties of the lowermost ~150 km of the mantle (the D″ layer) with this mineralogy. Here, using *ab initio* simulations and high-pressure experiments, we show that at pressures and

Figure 1 Structure of the post-perovskite phase of MgSiO3 (calculated at 120 GPa). SiO6 octahedra and Mg atoms (spheres) are shown. Similar structures are known for Fe2O3, CaIrO3, FeUS3, PbTlI3, UScS3, KTmI3, AgTaS3 and CaInBr3.

445